



## Improvement of Passive Vibration Damping of Satellite Solar Array Using Adaptive Boundary Conditions

E. Askar<sup>\*</sup>, E. Elsoaly<sup>†</sup>, M. Kamel<sup>‡</sup>, H. kamel<sup>§</sup>

**Abstract:** Satellite solar array structures experience several loads during deployment and in orbit operations. Such loads cause vibrations and can lead to premature failure or improper service operation, hence, solar arrays must be designed to attenuate these vibrations. In addition, solar arrays must be as light weight as possible, which renders their design process as a fairly complicated one. An innovative approach is presented in this paper for improving the passive vibration damping of solar arrays by using adaptive boundary conditions. A case study of a solar array is investigated where experimental testing and finite element technique are efficiently integrated. In addition, a new theoretical technique is developed to predict first and second vibration modes of the solar array. The results are used to study the effects of boundary conditions on the vibration response of the solar array. They clearly show that by only changing the way the solar array is fixed, vibration damping is successfully improved.

**Keywords:** Adaptive boundary conditions, SA vibration attenuation, cantilever plate Vibration, cantilever plate theoretical analysis.

### 1. Introduction

Vibration control of flexible structures is an important issue in many engineering applications, especially for the precise operation of aerospace systems such as satellite structures.

#### 1.1 Effect of Vibration on Satellite Structures

Flexible structures have low stiffness and damping ratio. Therefore, any excitation can lead to increase of vibration amplitude and settling time. These can cause fatigue, disturbance and poor operation of the structures [1]. Vibration of a structure at low frequencies is a challenging problem in light weight and flexible structure such as satellites SA structure [2]. SA structure is susceptible to several sources of vibration during deployment and in orbit operations such as: satellite maneuver, solar snap effect, and moving parts, as well as propulsion system.

Such sources of vibration cause instability of SA structure, due to the condition of resonance. Therefore, many types of vibration damping techniques are used in space structure applications.

#### 1.2 Vibration Damping Techniques

Vibration characteristics of many structures are influenced by the mass, stiffness, and damping of the structure. Both mass and stiffness influence the fundamental frequency of the structure, while damping reduces the peak amplitude of the structure [3].

Several methods are used in vibration control such as passive, active, and semi-active or hybrid vibration control. In a passive control system, the energy of vibration is dissipated by a

<sup>\*</sup> Egyptian Armed forces, Egypt, [emadaskar2@gmail.com](mailto:emadaskar2@gmail.com)

<sup>†</sup> Prof., Higher Tech. Institute, 10th of Ramadan, Egypt, [Dr.ELSOALY@hotmail.com](mailto:Dr.ELSOALY@hotmail.com)

<sup>‡</sup> Egyptian Armed forces, Egypt, [Kamelema\\_1971@hotmail.com](mailto:Kamelema_1971@hotmail.com)

<sup>§</sup> Egyptian Armed forces, Egypt, [hisham.kamel@mtc.edu.com](mailto:hisham.kamel@mtc.edu.com)

damping element without any feedback capability, while in an active system; a force is applied by using actuating elements as piezoelectric actuator in an equal and opposite direction to the force imposed by the external excitation. A hybrid method combines both approaches.

### 1.3 Passive Vibration Damping

Passive damping systems can be used in space structures due to their simplicity, capability of suppressing a wide range of mechanical vibrations, and no power consumption required. The physical effect of passive dampers is based on the dissipation of load induced energy. The reduction of the vibration level at a sensitive location of structure can be achieved by three approaches: at source, receiver, and along the vibration path.

At the source and receivers, these actions can be achieved by minimizing the vibration amplitude such as placing the equipment in appropriate mounting. Along the vibration path, this action can be achieved by modification of the structure element or re-location of equipment to reduce the mechanical coupling between source and receiver. All these approaches are considered from the passive damping techniques. An alternative passive vibration damping is treated using adaptive boundary conditions, to decrease SA structure transverse vibrations.

### 1.4 Satellite SA Structure Configurations:

Satellite structure can be divided into three parts:

- Primary structure: which is considered as the backbone of the satellite, because it resists and supports most critical load conditions, it consists of mechanical parts that holds the subsystem together.
- Secondary structure: Appendages such as: SA panels, antennas, fuel tanks.
- Tertiary structure: such as the mounting parts (brackets, connections, and supports).

According to this classification of spacecraft structures, SA panels is considered from the main secondary structure components. Its main purpose is to provide the needed area for solar cells, and maintain their integrity and stability under launch and in orbit loads [4].

Generally, SA panels are kept in the stowed condition while launching, and deployed after the satellite enters into its orbit. Deployment of these panels has considerable influence on dynamic and attitude control of satellite and may make disturbances. To prevent and minimize these disturbances in attitude control of a satellite, it is necessary to design SA panels and its deployment mechanism with appropriate performance and ability to control the disturbances.

SA used in satellites consists of a yoke or hinges connected on satellite primary structure with different boundary conditions [5,6], which usually consist of more than one panel according to the satellite configuration as shown in Fig. 1.

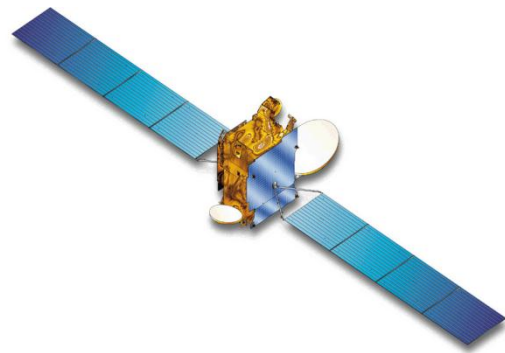
The dynamics of SA is influenced by many parameters (yoke/hinge fixation, panel flexibility, etc.) [7]. Hence, in our article we will concern with the effect of SA boundary conditions, on the amplitude frequency response function, when exposed to harmonic excitation.

### 1.5 Determination of Damping Ratio

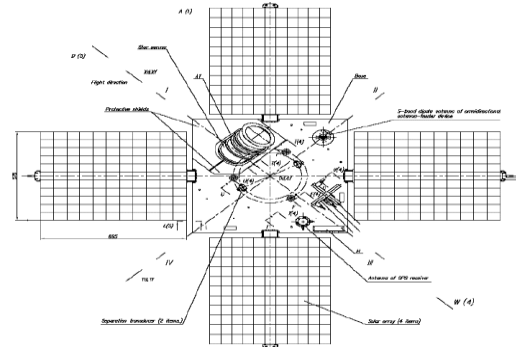
There are two main methods to measure the structure damping ratio ( $\zeta$ ) (zeta): half-power bandwidth method, and logarithmic decrement method [8, 9].

#### 1.5.1 Half-power bandwidth method

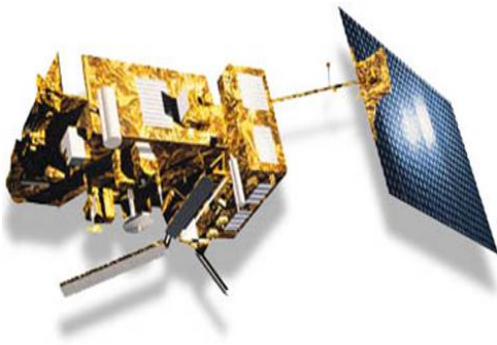
In this method, amplitude frequency response function (FRF) of the system is obtained. Corresponding to each natural frequency, there are peaks in amplitude FRF. 3dB (logarithmic scale) down from the peak there are two points corresponding to half power point. Structural loss factor  $\eta = 2\zeta$ .



Communication satellite



Remote sensing satellite



Research satellite



International space station (ISS)

**Fig. 1 Different SA boundary conditions and configurations**

In case of harmonic excitation, the damping ratio is measured by using the half power band width method, as shown in Fig. 2, and is given by the relation:

$$\zeta = \frac{\omega_2 - \omega_1}{2\omega_0} \quad (1)$$

Thus, by determining the two frequencies and at which the response is  $1/\sqrt{2}$  of the value from the resonant peak value  $X_{\max}$  and at the resonance frequency  $\omega_0$ , the damping ratio  $\zeta$  can be determine using the previous relation.

### 1.5.2 Logarithmic decrement method

Logarithmic decrement method is used to calculate damping ratio for damped system in time domain. It can be calculated from natural log of the ratio of the amplitudes of any successive peaks, as shown in Fig. 3.

This method has lower accuracy especially when damping ratio more than 0.5. The logarithmic decrement  $\delta$  can be calculated as:

$$\delta = \frac{1}{n} \ln \left| \frac{X_1}{X_{n+1}} \right| \quad (2)$$

where:  $X_n$ - is the  $n^{\text{th}}$  amplitude of oscillation

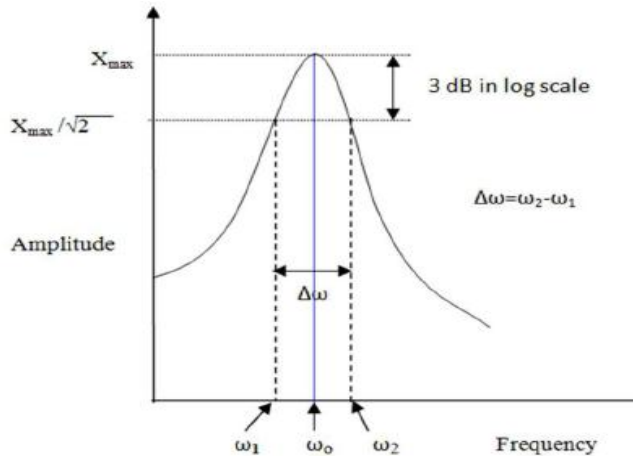


**Fig. 2 Half power bandwidth method [8, 9]**

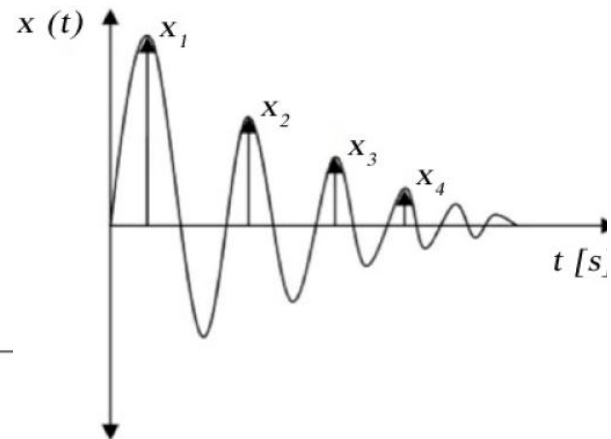


**Fig. 3 Logarithmic decrement method [8, 9]**

Damping ratio can be calculated as:

$$\zeta = \frac{\delta}{\sqrt{4\pi^2 + \delta^2}} \quad (3)$$

## 2. Modal Analysis

### 2.1 Test Specimen's Properties

Aluminum (5056) rectangular plate with pre-prepared different boundary condition (BC) configuration (single edge, double edge) as shown in Table 1. The dimensions of the plate are chosen based on the actual dimensions of satellites SA structure.

In Table 2, are given the dimensions and properties of the test specimen, used in the FE model analysis and experimental set up.

### 2.2 Finite Element Modeling of the System

FE model of a cantilever plate is done using ANSYS Workbench version R15.0. The structure discretized into smaller elements of identical shapes and sizes. The element numbers are decided after a convergence study made for the ANSYS model. Mesh sensitivity analysis is conducted to obtain accurate FE model, Fig. 4 shows the plate amplitude at different mesh size. The convergence is obtained at 5 mm element size at which the model contains 4036 elements and 28962 nodes, the element type is "solid 186" - 20 node homogenous structural solid. Static Structural analysis tool is performed to apply the plate gravity, and cantilever boundary conditions are applied to the FE model. Mode shapes and natural frequencies (NF) of the plate at different boundary conditions are obtained by modal analysis tool. Harmonic response tool was applied to study the plate amplitude frequency response function (FRF) for the first two bending modes.

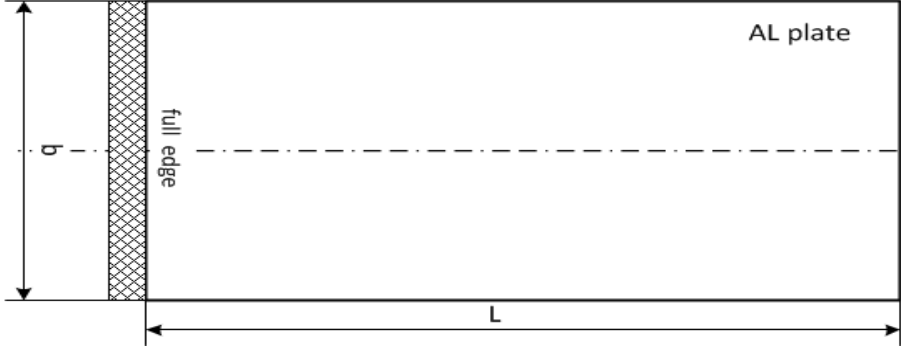
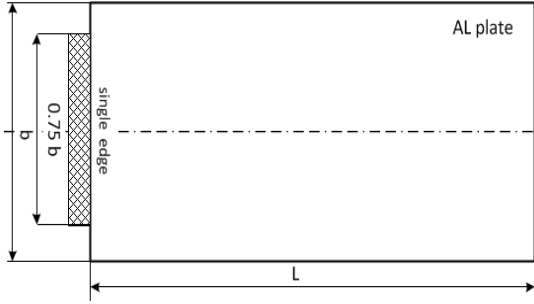
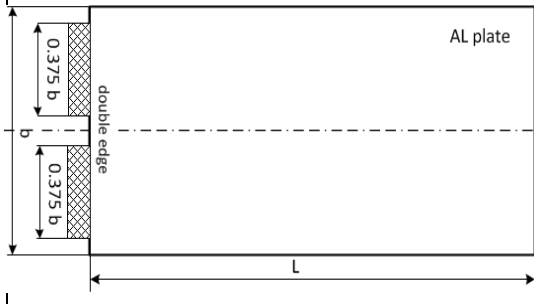
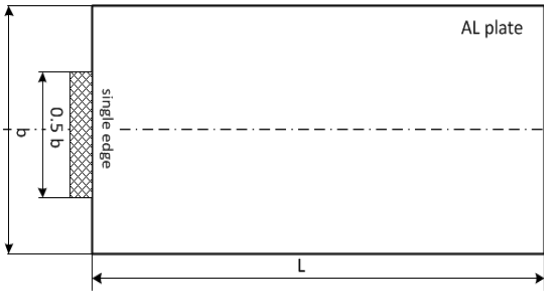
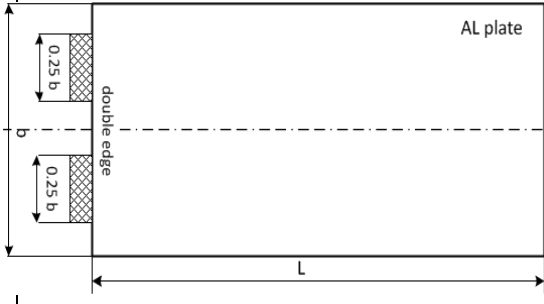
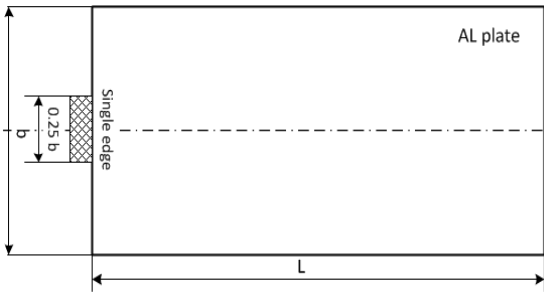
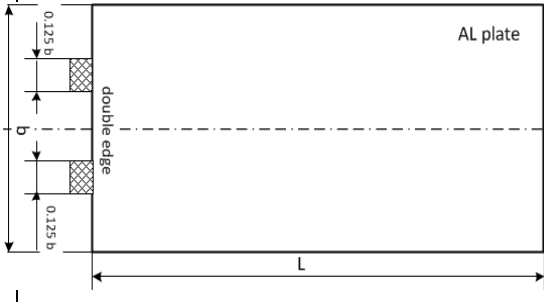
#### 2.2.1 Mode shapes of the plate with different boundary conditions

The first two bending mode shapes of the plate with different boundary conditions and aspect ratio 2.5, are shown in Fig. 5 and Fig. 6.

#### 2.2.2 Harmonic analysis

A harmonic response tool is applied to study the plate frequency response function (FRF) for the first two bending modes. It is carried out for the plate with different boundary conditions. A transverse excitation force of 1 N with frequency varies from 0 to 200 Hz is applied at the plate structure. FRF of a structure, otherwise called a transfer function is a ratio of the output signal to the input signal in frequency domain.

**Table 1 AL plate with different BC configurations: (a) single edge, (b) double edge**

| BC percentage | (a) Single edge BC1   | (b) double edge BC2  |
|---------------|---|--|
| 100%          |   |  |
| 75%           |   |   |
| 50%           |  |  |
| 25%           |  |  |

**Table 2 AL plate test specimens' technical properties**

| Material type | Dimensions (mm) | Young's modulus E (GPa) | Density $\rho$ (kg/m <sup>3</sup> ) | Poisson's ratio $\nu$ |
|---------------|-----------------|-------------------------|-------------------------------------|-----------------------|
| AL 5056       | (500x200x1.2)   | 70                      | 2660                                | 0.33                  |

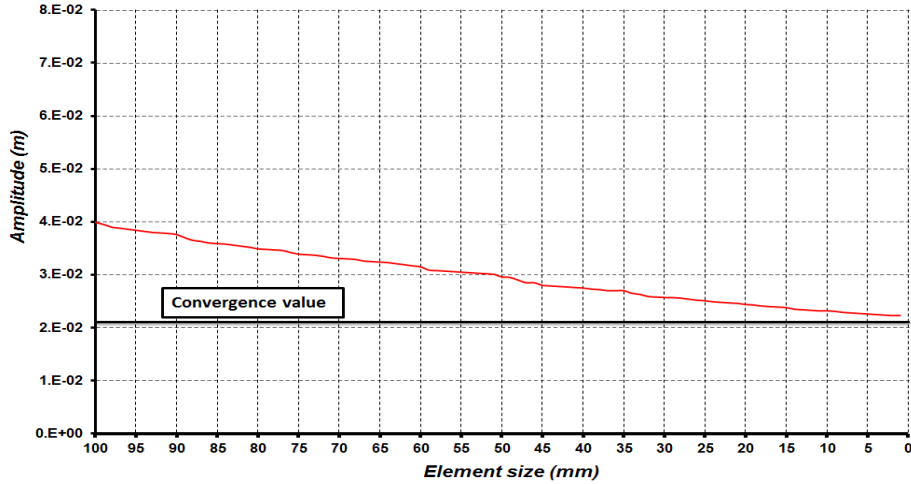


**Fig. 4 The plate amplitude at different mesh size**

### 3. Theoretical Analyses

#### 3.1 Cantilever Plate Natural Frequency Literature Survey

Warburton [10] used Rayleigh method to find the first angular frequency of a vibrating cantilever plate ( $\omega_1$ ) as:

$$\omega_1 = \frac{3.66}{L^2} \sqrt{\frac{D}{\rho}} \quad (4)$$

where:  $L$ ,  $\rho$ , and  $D$ , are the plate length, areal density and flexural rigidity per unit width respectively.

$$D = \frac{E t^3}{12(1 - \varepsilon^2)} \quad (5)$$

where:  $E$ ,  $t$ , and  $\varepsilon$ , are the plate modulus of elasticity, thickness, and Poisson's ratio respectively.

Dalley and Ripperger [10, 11] obtained the first and second angular frequencies for aluminum plate with aspect ratio 2.5 as:

$$\omega_1 = \frac{3.35}{L^2} \sqrt{\frac{D}{\rho}} \quad (6)$$

$$\omega_2 = \frac{15.5}{L^2} \sqrt{\frac{D}{\rho}} \quad (7)$$

#### 3.2 Determination of Plate Natural Frequency using Energy Method

When the tip deflection of a cantilever plate is maximum as shown in Fig. 7, all parts of plate are motionless. At that time, all the energy associated with vibration is in the form of elastic potential energy. When the plate is passing through its equilibrium position, all the vibrational energy will be in the form of kinetic energy.

The application of conservation of energy principle states that, the potential energy in the position of maximum deflection must equal to the kinetic energy when passing through the equilibrium position. Therefore, the following relation can be considered for vibration of elastic plate:

$$U_{\max} = T_{\max} \quad (8)$$

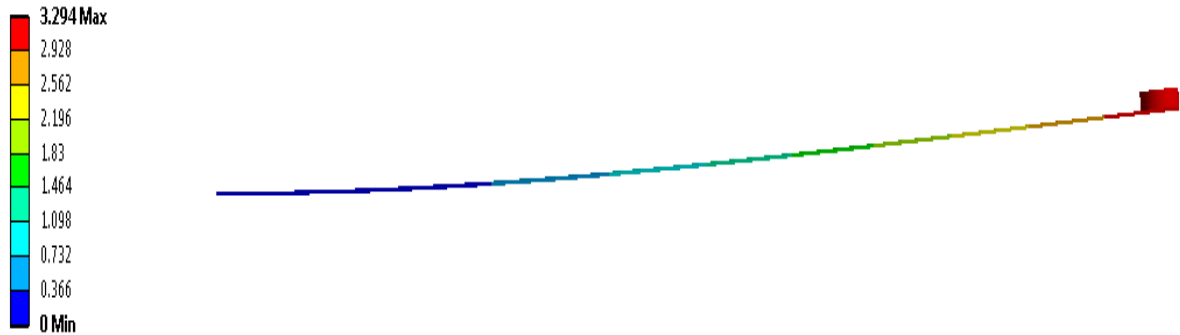
where:

$U_{\max}$  is the maximum value of potential strain energy,

$T_{\max}$  is the maximum value of kinetic energy.

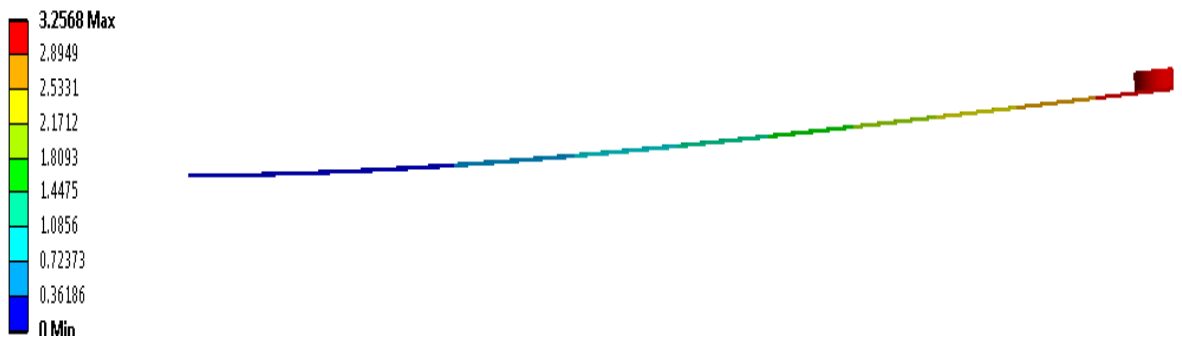
### First bending mode

Frequency: 3.768 Hz  
Unit: m  
8/30/2016 4:32 PM



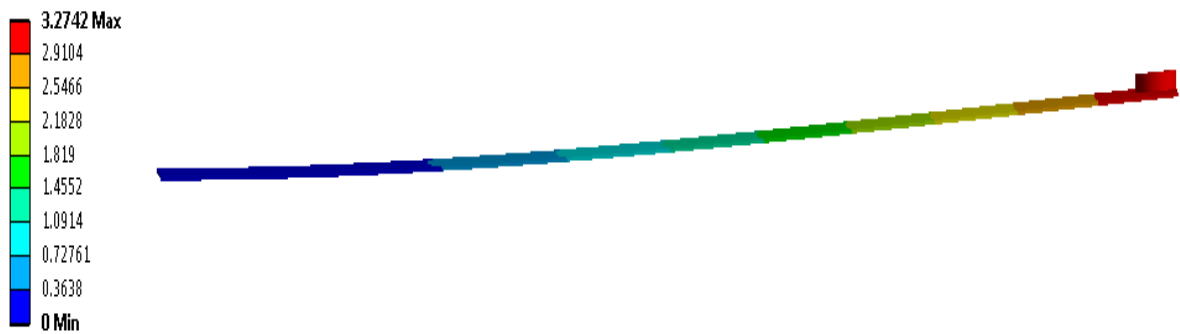
(a) Full BC

Frequency: 3.5683 Hz  
Unit: m  
10/1/2016 2:06 PM



(b) Single edge BC1

Frequency: 3.663 Hz  
Unit: m  
10/1/2016 2:12 PM

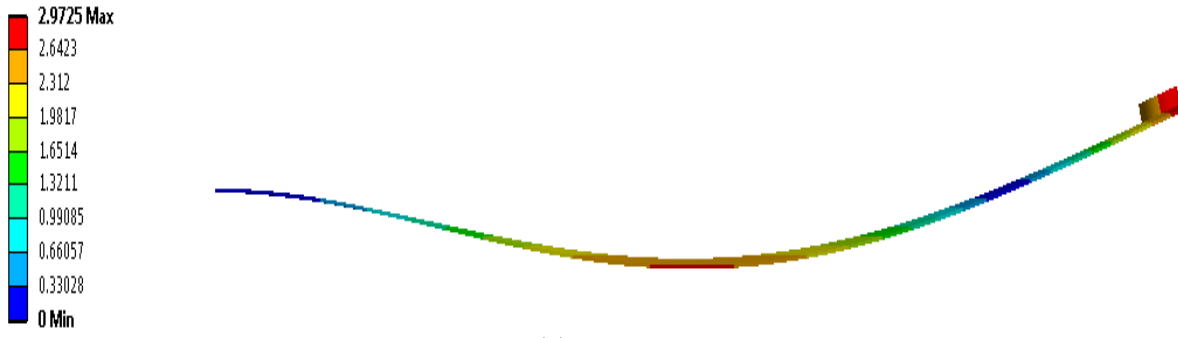


(c) Double edge BC2

**Fig. 5** The first bending mode shape of the plate with (a) Full, (b) Single edge, (c) Double edge boundary conditions

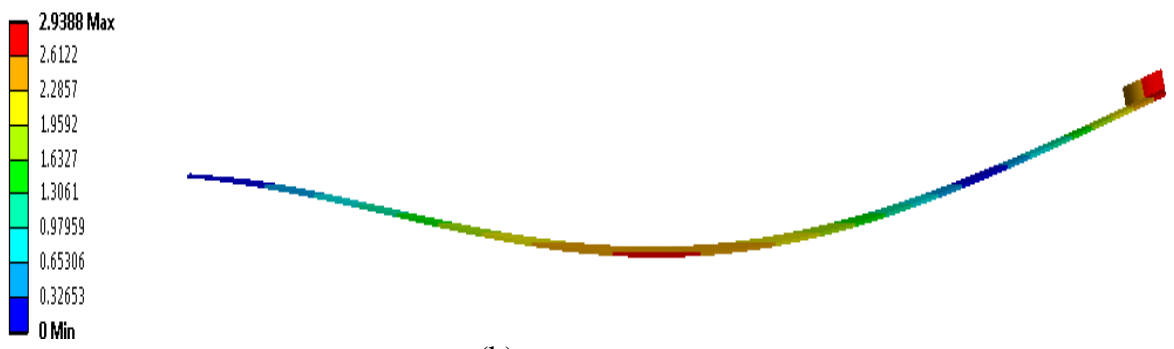
Second bending mode

Frequency: 23.926 Hz  
 Unit: m  
 8/30/2016 4:35 PM



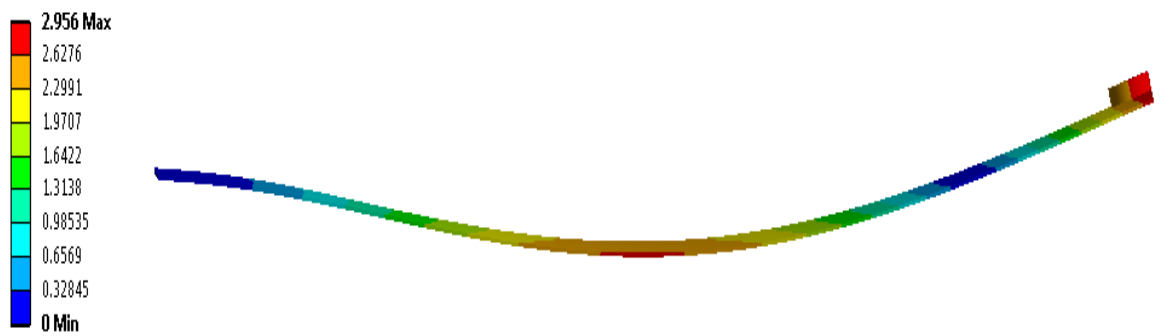
(a) Full BC

Frequency: 22.698 Hz  
 Unit: m  
 10/1/2016 2:07 PM



(b) Single edge BC1

Frequency: 23.28 Hz  
 Unit: m  
 10/1/2016 2:13 PM



(c) Double edge BC2

**Fig. 6** The second bending mode shape of the plate with (a) Full, (b) Single edge, (c) Double edge boundary conditions



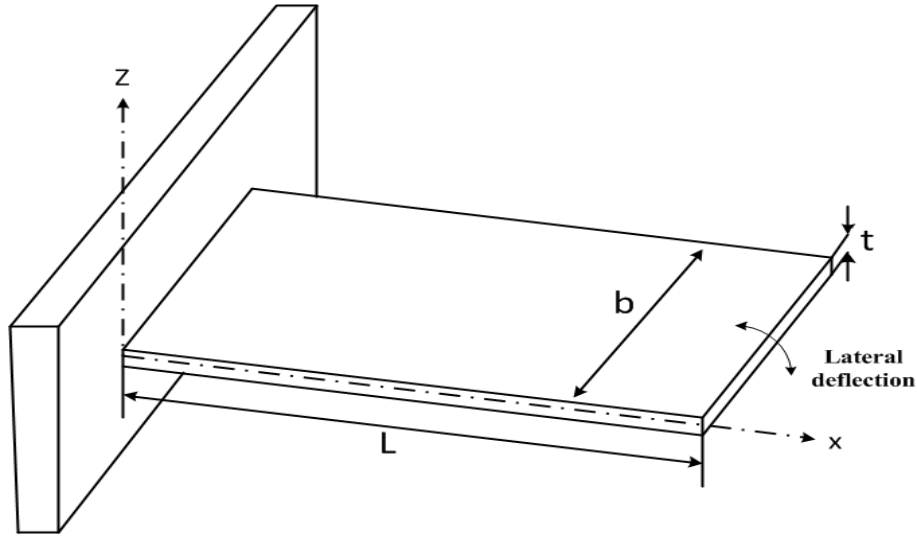


**Fig. 7 Cantilever plate**

The strain energy  $U$  of a uniform plate can be expressed in the form:

$$U = \frac{D}{2} \int_0^L Z''^2 dx \quad (9)$$

where:  $Z''$  is the second derivation of the plate lateral deflection  $Z$  with respect to  $x$  for each mode shape, and  $D$  is the plate flexural rigidity.

The kinetic energy  $T$  of a uniform plate can be expressed in the form:

$$T = \frac{\rho}{2} \int_0^L Z'^2 dx \quad (10)$$

where:  $Z'$  is the first derivation of the plate lateral deflection  $Z$  with respect to  $t$  for each mode shape, and  $\rho$  is the plate areal density.

If we consider the free vibration of a rectangular cantilever plate of length  $L$  and width  $b$  along  $x$  axis, so that the plate bends into a cylindrical surface, such behavior is called cylindrical bending at which the deflection in such condition is similar to the deflection of a bent beam, with this approximation the analysis will be considerably simplified.

### 3.2.1 First mode of vibration of uniform cantilever plate

The convenient expression for the lateral deflection  $Z$ , which satisfies the boundary conditions, may be assumed as:

$$Z = \Delta \left( 1 - \cos \frac{\pi x}{2L} \right) e^{\omega t} \quad (11)$$

where:

$\Delta$  - is the plate maximum deflection (at  $x=L$ ), and  $\omega$  is the plate angular frequency.

Substituting Eq. 11 into Eq. 9, the plate strain energy  $U$  is obtained, in the form:

$$U = \frac{D}{2} \Delta^2 \left(\frac{\pi}{2L}\right)^4 \int_0^L \cos^2 \frac{\pi x}{2L} e^{2\omega t} dx \quad (12)$$

Substituting Eq. 11 into Eq. 10, the plate kinetic energy T is obtained as:

$$T = \frac{1}{2} \rho \int_0^L \left[ \Delta \left(1 - \cos \frac{\pi x}{2L}\right) \omega e^{\omega t} \right]^2 dx \quad (13)$$

Substituting Eq. 12 and Eq. 13 into Eq. 8, and performing the integration, the following relation is reached:

$$\frac{D}{64} \Delta^2 \frac{\pi^4}{L^3} = 0.1137 \rho \Delta^2 \omega^2 \quad (14)$$

Consequently the plate first angular frequency  $\omega_1$  will be:

$$\omega_1 = 3.66 \sqrt[2]{\frac{D}{\rho L^4}} \quad (15)$$

which is in convergence to the angular frequency, obtained from the classical transverse vibration analysis given in the literature as in Eq. 4, and Eq. 6.

### 3.2.2 Second mode of vibration of uniform cantilever plate

An expression for lateral deflection Z of cantilever plate, which satisfies the boundary conditions, may be assumed as:

$$Z = \Delta e^{-\frac{3\pi x}{2L}} \sin \frac{3\pi x}{2L} e^{-\omega t} \quad (16)$$

where:  $\Delta$  is constant, and L,  $\omega$ , x, and t are the plate length, angular frequency, longitudinal coordinate, and time variable respectively.

Considering Eq. 16, the second derivative of the lateral vibration variable Z, is obtained as:

$$Z'' = \Delta \left(\frac{3\pi}{2L}\right)^2 e^{-\omega t} e^{-\frac{3\pi x}{2L}} \cos \frac{3\pi x}{2L} \quad (17)$$

Substituting Eq. 16 into Eq. 9, we obtain the plate strain energy as:

$$U_{\max} = \frac{1}{24} D \Delta^2 \left(\frac{3\pi}{2L}\right)^4 \left(\frac{L}{\pi}\right) e^{-2\omega t} \quad (18)$$

Considering Eq. 16, the velocity function of vibration is obtained as:

$$Z' = -\Delta \omega e^{-\frac{3\pi x}{2L}} \cos \frac{3\pi x}{2L} e^{-\omega t} \quad (19)$$

Substituting Eq. 19 into Eq. 10, leads to:

$$T_{\max} = \frac{1}{8} \rho \omega^2 \Delta^2 \frac{L}{\pi} e^{-2\omega t} \quad (20)$$

Substituting Eq. 18 and Eq. 20 into Eq. 8 leads to:

$$\frac{1}{8} \rho \omega^2 = \frac{1}{24} D \left( \frac{3\pi}{2L} \right)^4 \quad (21)$$

Hence, the plate second mode natural frequency  $\omega_2$  is obtained in the form:

$$\omega_2 = \frac{12.82}{L^2} \sqrt[2]{\frac{D}{\rho}} \quad (\text{rad/s}) \quad (22)$$

which is in convergence to the angular frequency, obtained from the classical transverse vibration analysis given in the literature as in Eq. 7.

#### 4. Experimental Setup

The experimental set up consists of: commercially available 99% pure aluminum rectangular plate type (5056), with one end clamped in a fixed support and the other end is free. Fig. 8 and Fig. 9 show a schematic view and experimental setup component respectively. The tested plate is attached to B&k (Bruel& Kjaer) shaker type 4808 which excites the tested plate by sine sweep signal (0-200) Hz. The shaker is driven by B&k power amplifier (PA) type 2712 which amplifies the sine sweep function coming from NI PXIe-6368& NI SCB-68A system through Lab VIEW program.

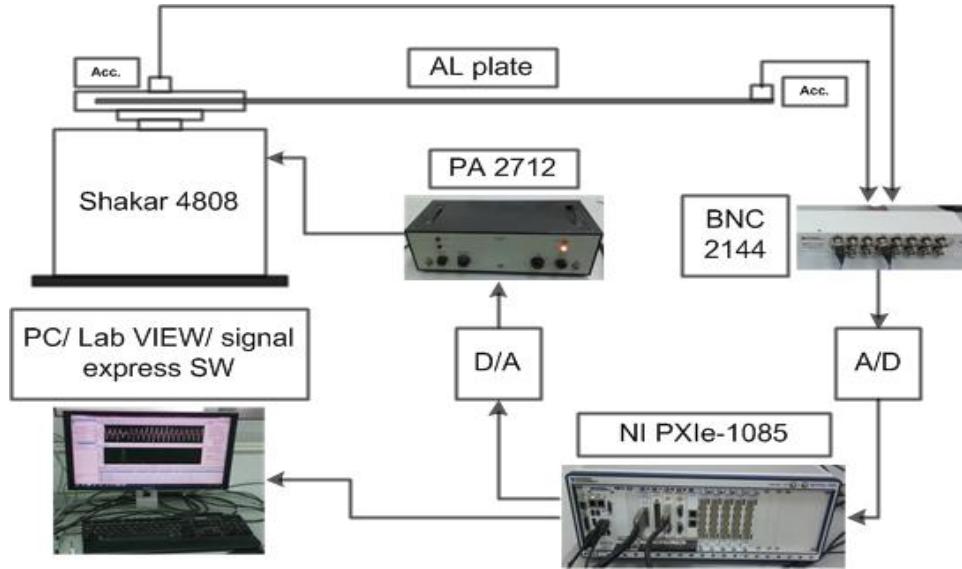


**Fig. 8 A schematic view of experimental setup**

The vibration amplitude depends, mainly, on the voltage applied to the shaker. Chasses of National Instrument (NI) type PXIe-1085 is used for data acquisition system. Two accelerometers type PCB PIEZOTRONICS are bonded on the host structure by a suitable adhesive, one in the proximity of the fixed end, and the other at the tip of the plate. The output signals are sent to NI adapter type BNC-2144 which is connected to analogue input NI PXIe-4499. A PC with Lab VIEW signal express 2015 SW is used to acquire and analysis the data. To obtain exact experimental results, ten repeated measurement are recorded for each experimental set up and the average values are applied for final results.

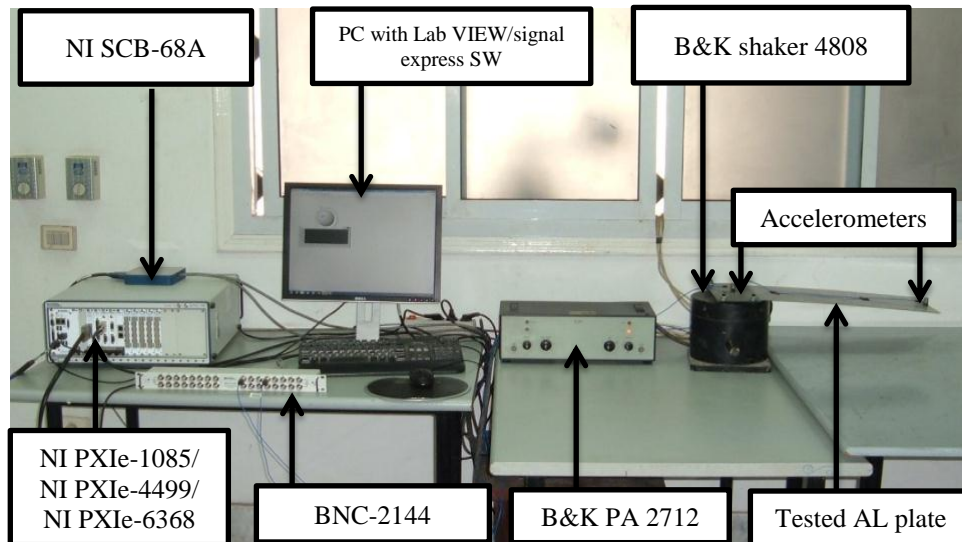


**Fig. 9 The experimental setup component**

## 5. Results and Discussion

### 5.1 Finite Element Modeling Verification

FE model results are compared with the experimental and theoretical ones.

Fig. 10 and Fig. 11 show the numerical and experimental FRF of the plate for the first and second bending modes with different plate boundary conditions (full, single, double) at aspect ratio = 2.5 respectively.

For different boundary conditions, the comparison between the resonant frequencies of the numerical simulation, experimental, and theoretical results, are given in Table 3.

The results show that the experimental and finite element model results are in a good agreement, where maximum error within (14 %). This error is due to the next hypotheses:-

- The simulated material properties of the plate aren't exactly as the AL plate specimen properties.
- The effect of the accelerometer placement on the plate and its fixation by wax material.
- The change in environmental conditions during tests (temperature, vibration, etc.).
- The attachment of the shaker with the AL plate isn't identical with the simulation.

### 5.2 Parametric Study

A parametric study is conducted to compare between the plate FRF with full boundary conditions and the plate FRF with (single, double) boundary conditions percentages at different plate aspect ratio. The study is applied for first and second bending modes.

The results of a parametric study are described as follow:

#### 5.2.1 The plate amplitude FRF at different single edge boundary condition (75%, 50%, 25%) and different plate aspect ratios.

The plate with different single boundary conditions is shown in Table 1. The plate amplitude FRF with different single boundary conditions and aspect ratio = 2 is shown in Fig. 12

## 5.2 Parametric Study

A parametric study is conducted to compare between the plate FRF with full boundary conditions and the plate FRF with (single, double) boundary conditions percentages at different plate aspect ratio. The study is applied for first and second bending modes.

The results of a parametric study are described as follow:

### 5.2.1 The plate amplitude FRF at different single edge boundary condition (75%, 50%, 25%) and different plate aspect ratios.

The plate with different single boundary conditions is shown in Table 1. The plate amplitude FRF with different single boundary conditions and aspect ratio = 2 is shown in Fig. 12

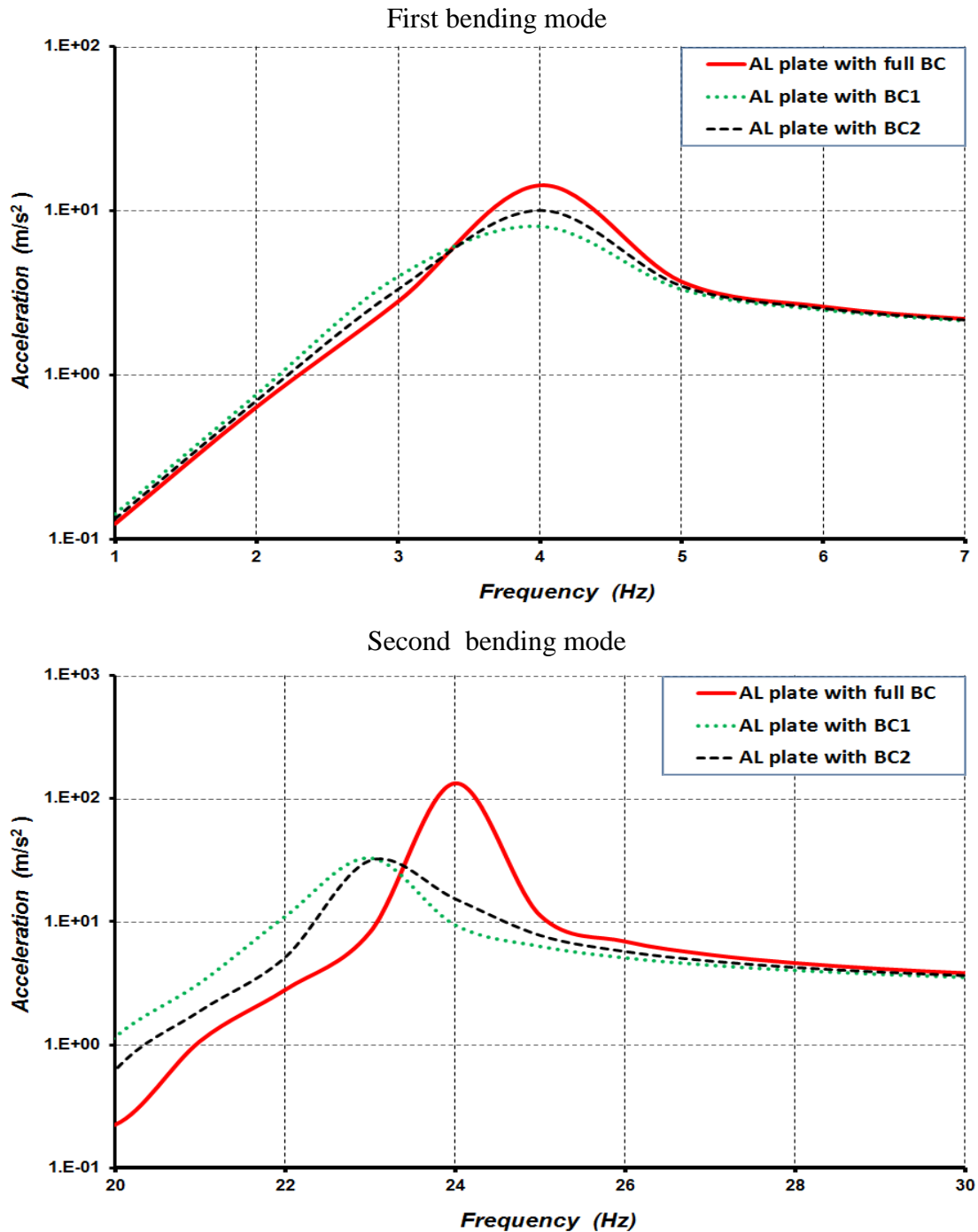
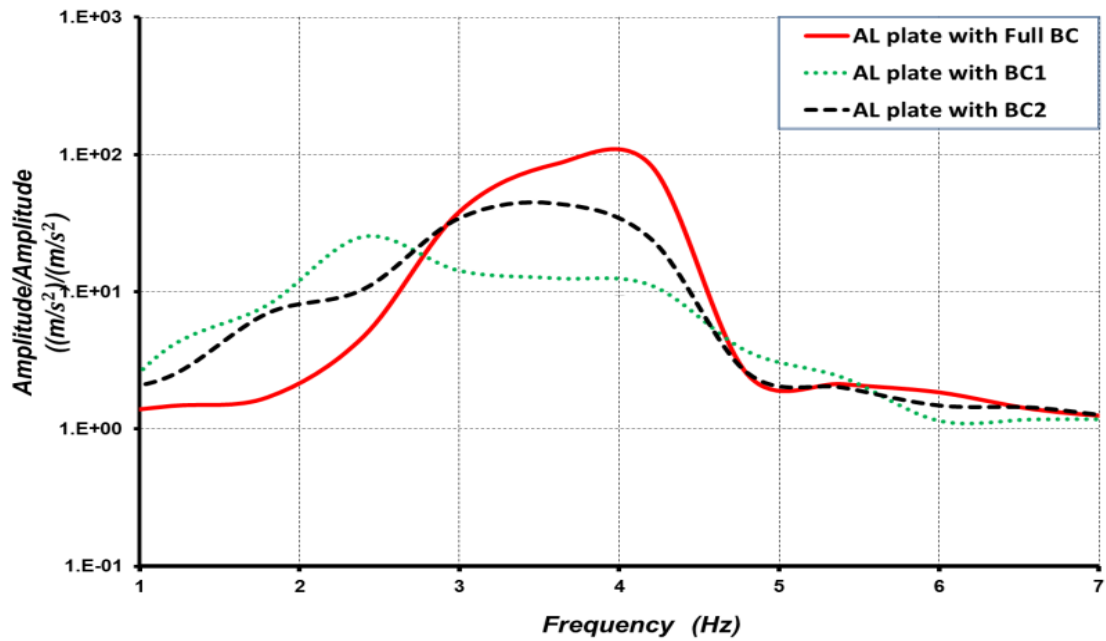


**Fig. 10** The numerical FRF of the plate with different plate boundary conditions (full, single, double) at aspect ratio = 2.5

## First bending mode



## Second bending mode

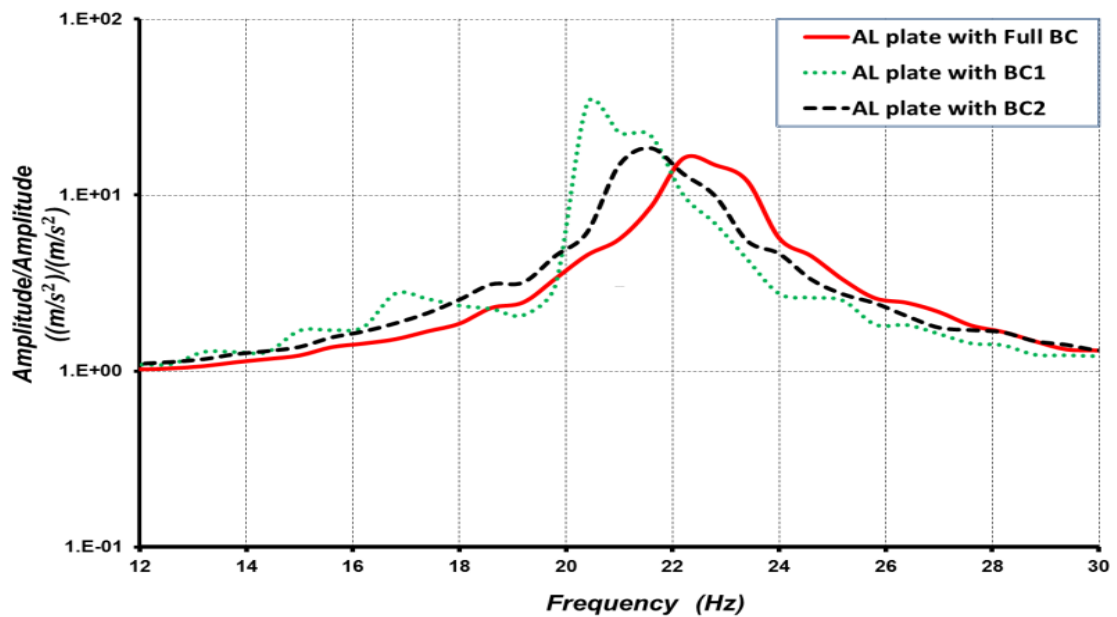


**Fig. 11** The experimental FRF of the plate with different plate boundary conditions (full, single, double) at aspect ratio = 2.5

**Table 3** The Plate Resonant Frequencies for Different Boundary Conditions (Numerically/Experimentally)

| Mode | The plate Resonant frequencies (Hz) |      |       |                                |      |                                |      |
|------|-------------------------------------|------|-------|--------------------------------|------|--------------------------------|------|
|      | Full clamped boundary condition     |      |       | Single edge boundary condition |      | Double edge boundary condition |      |
|      | Num.                                | Exp. | Theo. | Num.                           | Exp. | Num.                           | Exp. |
| 1    | 3.77                                | 3.6  | 4.34  | 3.59                           | 4.2  | 3.66                           | 4.2  |
| 2    | 23.93                               | 22.2 | 18.38 | 22.84                          | 21.6 | 23.28                          | 23.4 |

## 5.2 Parametric Study

A parametric study is conducted to compare between the plate FRF with full boundary conditions and the plate FRF with (single, double) boundary conditions percentages at different plate aspect ratio. The study is applied for first and second bending modes.

The results of a parametric study are described as follows:

### 5.2.1 The plate amplitude FRF at different single edge boundary condition (75%, 50%, 25%) and different plate aspect ratios.

The plate with different single boundary conditions is shown in Table 1. The plate amplitude FRF with different single boundary conditions and aspect ratio = 2 is shown in Fig. 12

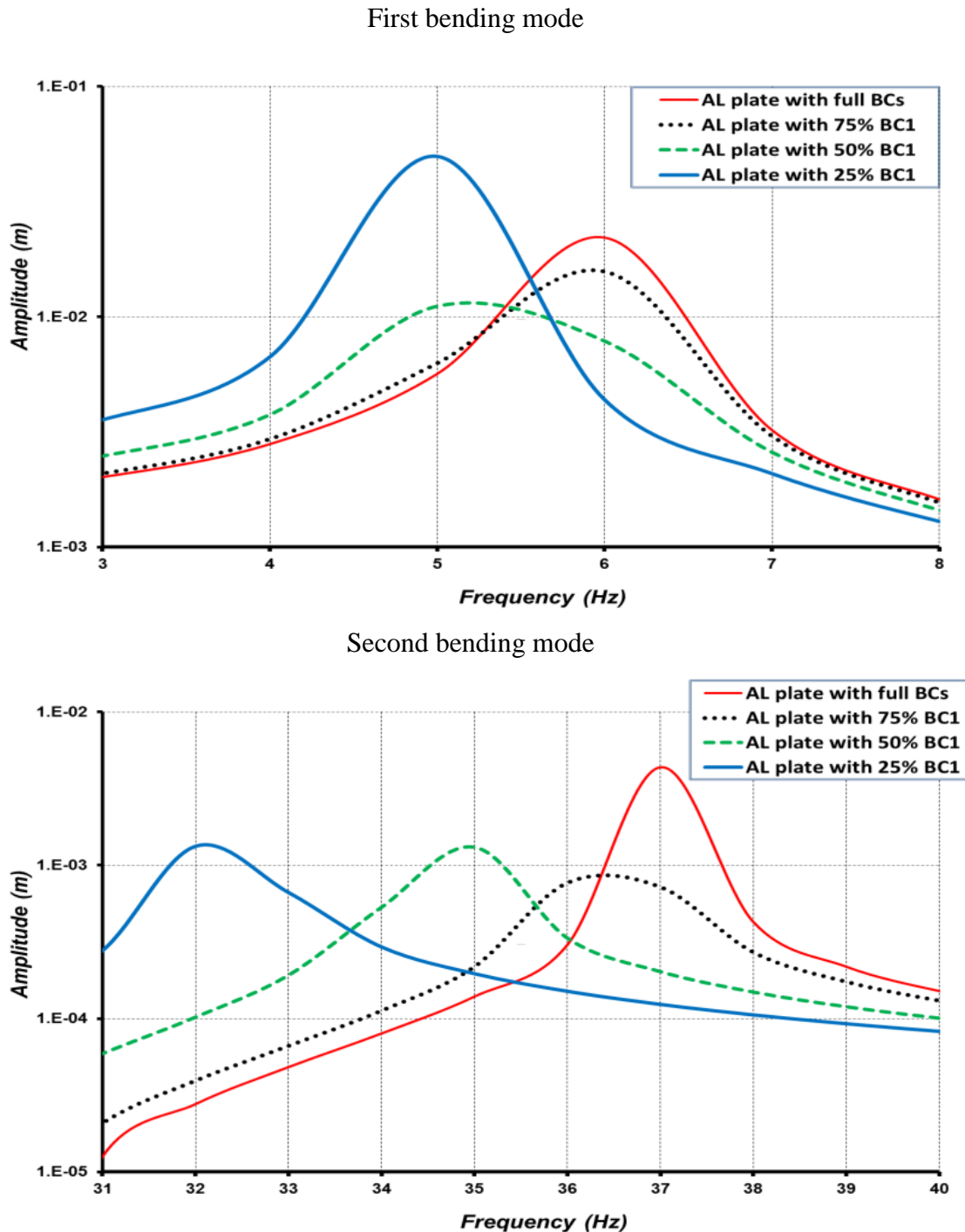


**Fig. 12** The plate amplitude FRF with different single edge boundary conditions and aspect ratio = 2

The plate amplitude FRF with different single edge boundary conditions and aspect ratio = 2.5 is shown in Fig. 13.

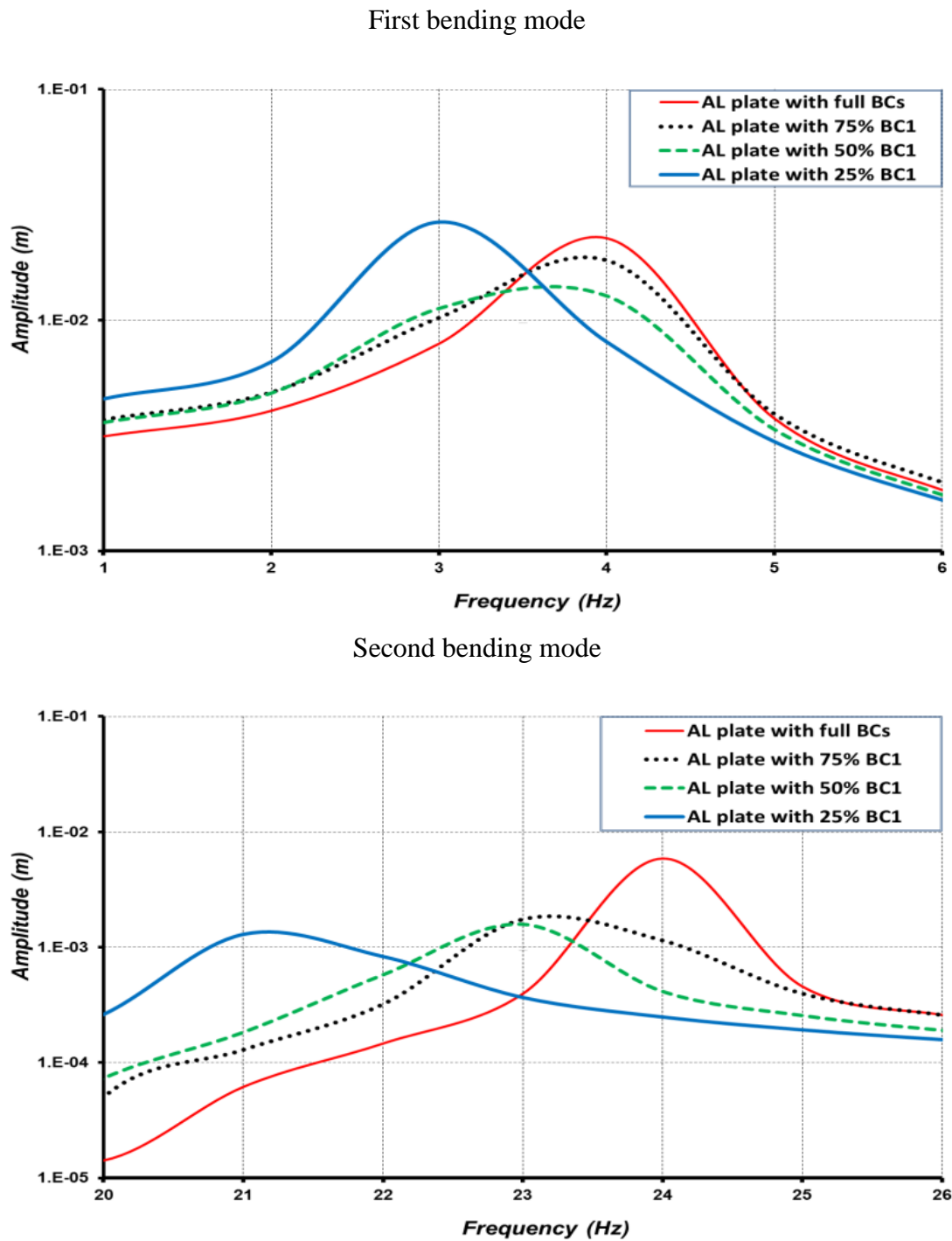


**Fig. 13** The plate amplitude FRF with different single edge boundary conditions and aspect ratio = 2.5



The plate amplitude FRF with different single boundary conditions and aspect ratio = 3 is shown in Fig. 14.

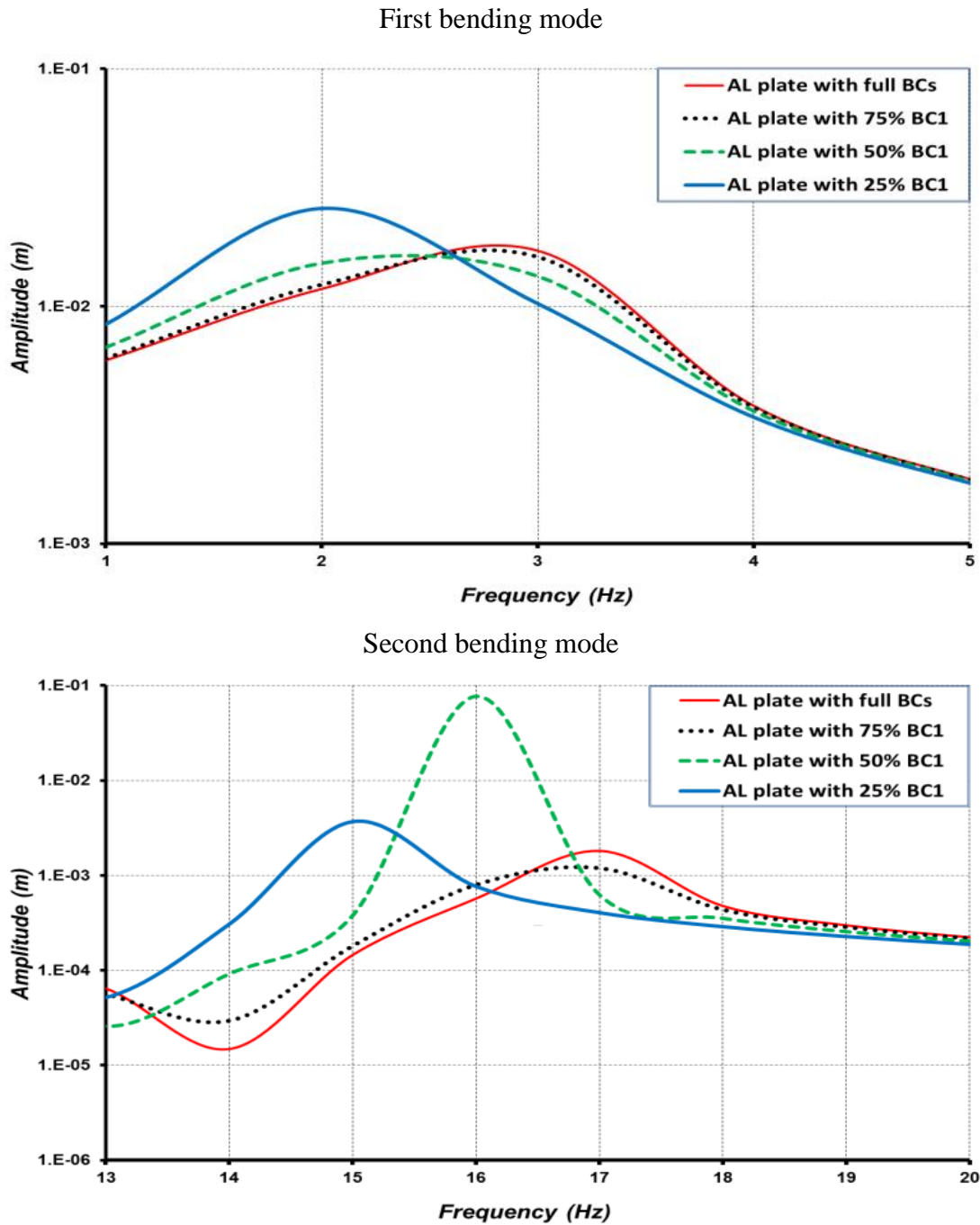


**Fig. 14** The plate amplitude FRF with different single edge boundary conditions and aspect ratio = 3

The results show that there is a significant decrease of the plate transverse amplitude and resonant frequency for single edge boundary conditions with (75%, and 50%) at plate aspect ratio (2, 2.5), compared to the full boundary condition one.

### 5.2.2 The plate amplitude FRF at different double edge boundary condition (75%, 50%, 25%) and different plate aspect ratios.

The plate with different double edge conditions is shown in Table 1. The plate amplitude FRF with different double boundary conditions and aspect ratio = 2 is shown in Fig. 15.

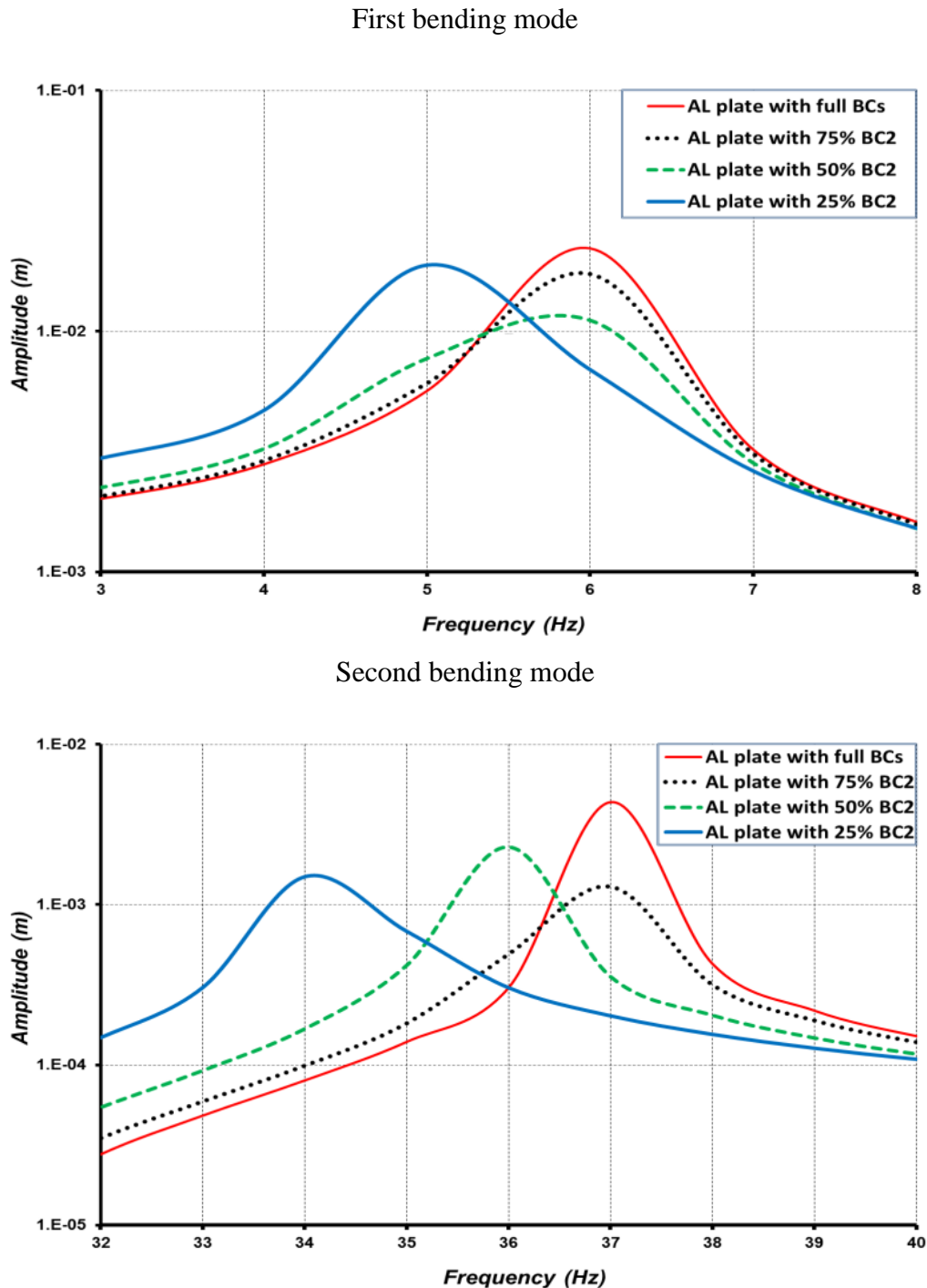


**Fig. 15** The plate amplitude FRF with different double edge boundary conditions and aspect ratio = 2

The plate amplitude FRF with different double boundary conditions and aspect ratio = 2.5 is shown in Fig. 16.

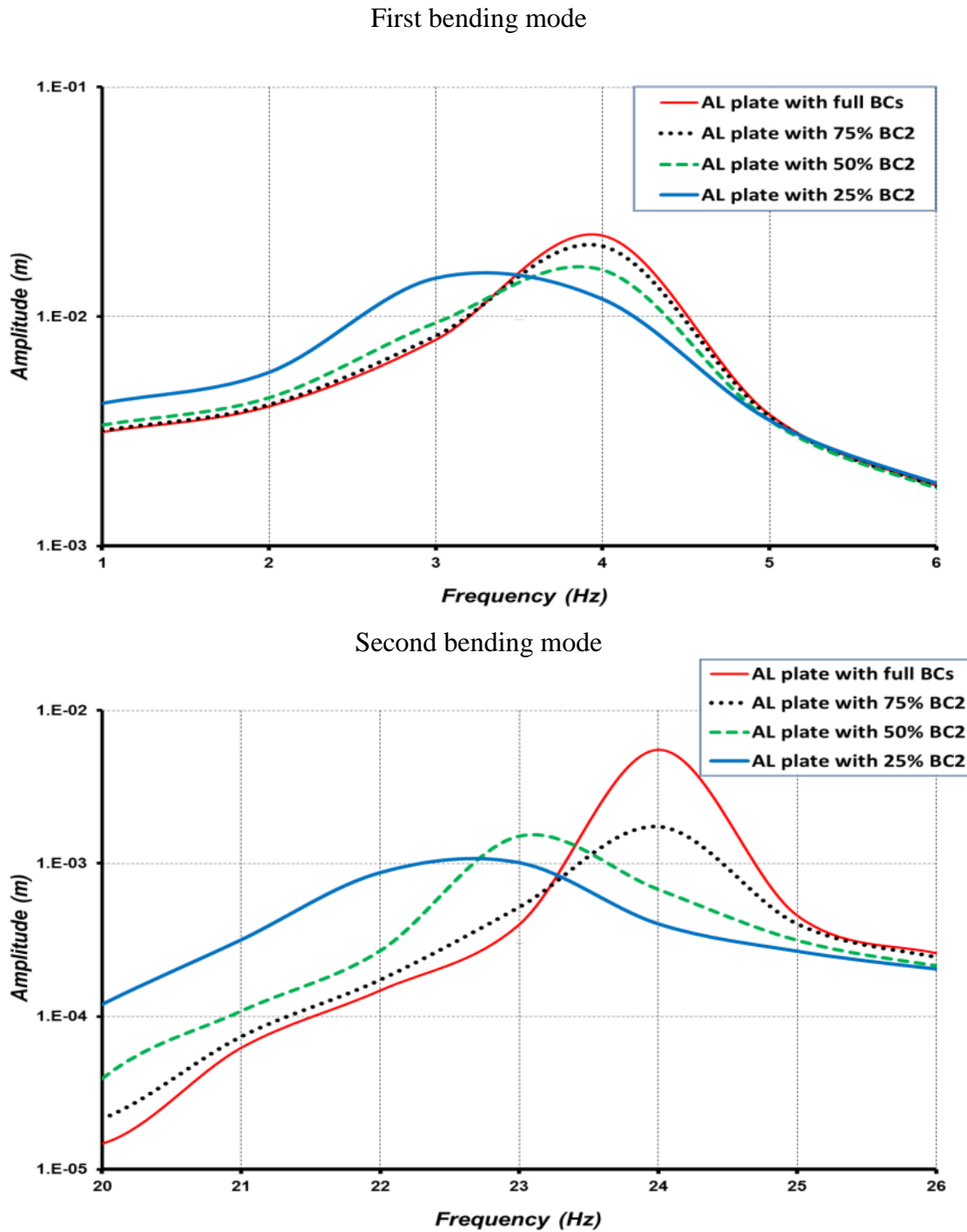


**Fig. 16** The plate amplitude FRF with different double edge boundary conditions and aspect ratio = 2.5

The plate amplitude FRF with different single edge boundary conditions and aspect ratio = 3 is shown in Fig. 17.

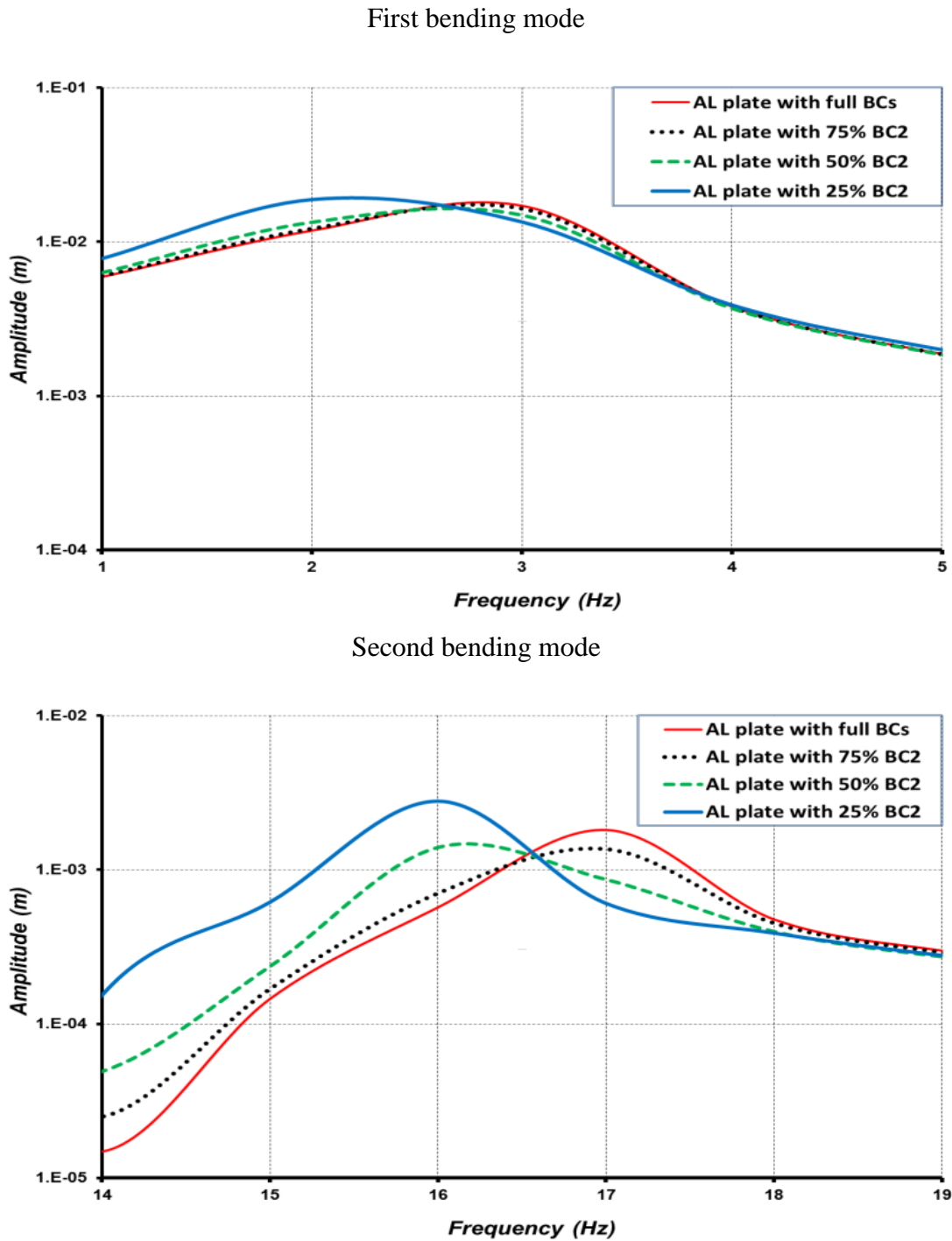


**Fig. 17** The plate amplitude FRF with different double edge boundary conditions and aspect ratio = 3

The results show that there is a significant decrease of the plate transverse amplitude and resonant frequency for double edge boundary conditions with (75%, and 50%, 25%) from the plate length at plate aspect ratio (2, 2.5) especially for the second mode, compared to the full clamped one.

## 6. Conclusions

It can be concluded from numerical, and experimental results that:

- Adaptive SA boundary conditions are remarkably effective in attenuating SA transverse vibration within a broad frequency range, especially for the first and second bending modes at single and double edge boundary conditions and plate aspect ratio less than 3, compared with full clamped boundary condition BC.
- Single edge boundary conditions BC1 with aspect ratio 2 and 2.5 achieve lower resonant frequency compared with double edge boundary conditions BC2.
- As SA aspect ratio increases more than 2.5, there is no significant decrease of SA transverse vibration when using single/double boundary conditions.

## 7. References

- [1] S. Havaldar, R. Sharma, V. Raghupathy and M. Adiga "evaluation of dynamic parameters of adhesively bonded steel and aluminum plates", ARPN Journal of Engineering and Applied Sciences, 2012.
- [2] V. Tatavolu and S. Panchumarthy, "embedded computer based active vibration control system for vibration reduction of flexible structures" Journal of Computer Science, ISSN: 1549-3636, 2013.
- [3] K. Sasikumar "experimental investigations of the effect of constraining layer parameters in vibration control of structures" International Journal of Advanced Research in Engineering and Applied Sciences, ISSN: 2278-6252, 2015.
- [4] O. Safak "Structural Design and Analysis of a Solar Array Substrate for a GEO Satellite" Master in Aerospace Science and Technology MAST 2013.
- [5] Sreejith, Vishnu, and Akhil "Supply Chain Management of Satellite Mechanisms- Product Development and Monitoring" Int. Journal of Engineering Research and Applications, 2014.
- [6] Birhanu F., Chen Z., and Ma W. "Modeling and simulation of satellite solar panel deployment and locking" information technology journal, ISSN 1812-5638, China, 2010.
- [7] B. Lakshmi , G. Sharma, G. Nagesh, C.D. Sridhara, and R. Ranganath "Analytical Estimation and Experimental Validation of Acceleration at Spacecraft Solar Array Latch-up Considering Differential Latching " Springer, India, 2015.
- [8] Yi Liu " Damping Technologies for Automotive Panel Structures " China, A thesis of Doctor of Philosophy 2011.
- [9] M. Jovanovic, A. Simonovic, N. Lukic, N. Zoric, S. Stupar, and S. Ilic "Experimental determination of active structure damping ratio using Different control strategies in system Of active vibration control" 6th international scientific conference on defensive technologies, Belgrade, OTEH 2014.
- [10] Arthur W. Leissa "Vibration of plates" Hand Book, NASA SP-160, Washington, DC, 1969, pp. 43,44,81.
- [11] J. Soovere "Aerospace structures technology -damping design guide" volume II, Ohio, 1985, pp 3-17,3-18.